ACS central science

http://pubs.acs.org/journal/acscii

Research Article

HaloFlippers: A General Tool for the Fluorescence Imaging of Precisely Localized Membrane Tension Changes in Living Cells

Karolína Straková,[§] Javier López-Andarias,*[,§] Noemi Jiménez-Rojo, Joseph E. Chambers, Stefan J. Marciniak, Howard Riezman, Naomi Sakai, and Stefan Matile*

Cite This: *ACS Cent. Sci.* 2020, 6, 1376−1385

Read Online

ACCESS | Metrics & More | Article Recommendations | Supporting Information

ABSTRACT: Tools to image membrane tension in response to mechanical stimuli are badly needed in mechanobiology. We have recently introduced mechanosensitive flipper probes to report quantitatively global membrane tension changes in fluorescence lifetime imaging microscopy (FLIM) images of living cells. However, to address specific questions on physical forces in biology, the probes need to be localized precisely in the membrane of interest (MOI). Herein we present a general strategy to image the tension of the MOI by tagging our newly introduced HaloFlippers to self-labeling HaloTags fused to proteins in this membrane. The critical challenge in the construction of operational HaloFlippers is the tether linking the flipper and the HaloTag: It must be neither too taut nor too loose, be hydrophilic but lipophilic enough to passively diffuse across membranes to reach the HaloTags, and allow partitioning of flippers into the MOI after the reaction. HaloFlippers with the best tether show localized and selective fluorescence after reacting with HaloTags that are close enough to the MOI but remain nonemissive if the MOI cannot be reached. Their fluorescence lifetime in FLIM images varies depending on the nature of the MOI and responds to myriocin-mediated sphingomyelin depletion as well as to osmotic stress. The response to changes in such precisely localized membrane tension follows the validated principles, thus confirming intact mechanosensitivity. Examples covered include HaloTags in the Golgi apparatus, peroxisomes, endolysosomes, and the ER, all thus becoming accessible to the selective fluorescence imaging of membrane tension.

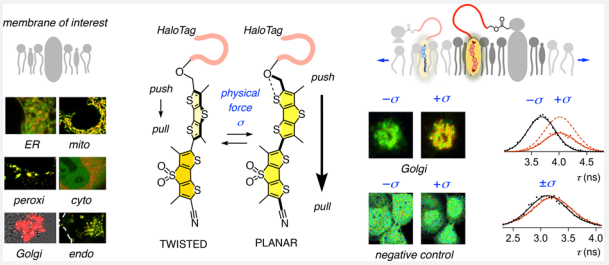

INTRODUCTION

Mechanobiology, or the study of how living organisms respond to mechanical stimuli, is a field full of challenges that have just started to emerge.[1−4] One of the reasons for the reluctant emergence of mechanobiology is the lack of routine small-molecule chemistry tools to image physical forces in living systems. The difficulty in creating such mechanosensitive probes is understandable because Newton's apple has already taught us, in the midst of the 1665 Great Plague confinement, that not the forces as such but only their consequences can be seen. The challenge to image the tension applied to biomembranes with general, user-friendly small-molecule fluorescent probes has recently been addressed with mechanosensitive "molecular flippers".[5−8] Flipper probes report quantitatively on tension by responding to the consequences in biomembrane architecture, including lipid decompression but mostly reorganization (Figure 1A).[5] First indications of the functional consequences of tension-induced microdomain assembly and disassembly have already been identified with regard to signal transduction, that is, the activation of TORC2,[9,10] thus providing a perfect illustration of the impact of physical forces on biological function.

Flipper probes have been rigorously engineered and tailored over the years, with **1** being the optimal design, commercially known as Flipper-TR (Figure 1D).[5,8] Flipper-TR is a planarizable push−pull probe. It is built around two dithienothiophene "flippers"[11,12] that are twisted out of coplanarity due to repulsion between the methyl groups and σ holes on sulfur atoms at opposite sides of the connecting twistable bond.[6,13,14] Polarization of the probe is initiated by endocyclic sulfide and sulfone bridges in the donating and accepting flippers. They are supported by an exocyclic cyano acceptor and more complex but essential ether donors that turn on only once the flipper planarization strengthens the electron-donating chalcogen bond.

In the twisted form in apolar solvents, the absorption and excitation maxima of flipper **1** are blue-shifted. In water, fluorescence is fully quenched, which is important for minimizing background and artifacts in bioimaging. Mechanical planarization in membranes of increasing order brings the two flippers into conjugation. This turns on the push−pull

Received: May 24, 2020
Published: July 20, 2020

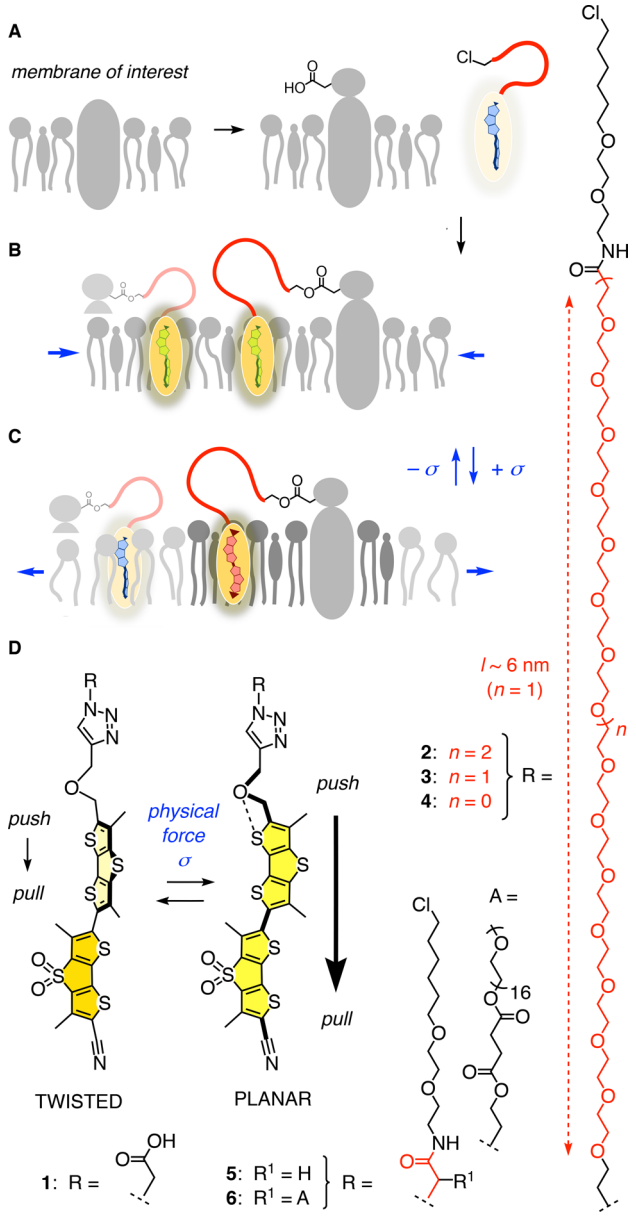

Figure 1. (A–C) Design of HaloFlippers to image membrane tension in the membrane of interest (MOI). (D) Structure and molecular mechanism of Flipper-TR **1** and HaloFlippers **2**–**6**. The estimated tether length (l) is of the fully stretched conformer. (A) A HaloTag is fused to a protein in the MOI. (B) Chloroalkanes of HaloFlippers react with the HaloTag to label the MOI. (C) HaloFlippers report the tension σ applied to the MOI as increasing lifetime τ because the response is dominated by the planarized flippers in the ordered microdomains produced by tension-induced phase separation (red) rather than the deplanarized flippers in the decompressed membrane (blue). (D) Planarization of the twisted flippers in equilibrium in the ground state turns on the push–pull system, red shifts excitation maxima, and increases fluorescence lifetimes.

dipole, shifts the excitation maximum up to almost 100 nm to the red, from 421 to 519 nm, and increases the fluorescence intensity and lifetime. The emission maximum around 600 nm is nearly mechano-insensitive because the emission always occurs from a fully planarized excited state.[6] This combination of planarization and polarization in equilibrium in the ground state often occurs in nature, from lobster pigmentation[15−17] to the chemistry of vision,[18−20] but is unexplored in the design of fluorescent probes. Most other fluorescent membrane probes operate in the excited state by different mechanisms, such as intramolecular charge transfer (ICT), twisted intramolecular charge transfer (TICT), excited-state intramolecular proton transfer (ESIPT), photoinduced electron transfer (PET), Förster resonance energy transfer (FRET), and the like.[21−28]

Changes in flipper lifetimes upon planarization/deplanarization allow us to image membrane tension using concentration-independent fluorescence lifetime imaging microscopy (FLIM). In multicomponent model membranes and biomembranes, the application of tension by micropipette aspiration or osmotic stress causes a linear increase in flipper lifetime. This is consistent with the dominant response from tension-induced membrane reorganization.[5,29−32] With increasing tension, unstretchable lipids are sorted out in highly ordered microdomains with fully planarized flippers with high oscillator strength and lifetime (Figure 1A). Disassembly of these microdomains with decreasing tension then causes the corresponding decrease in lifetime.

The carboxylic acid at the terminus of amphiphile **1** serves as an anchoring group in the plasma membrane (Figure 1D). Substitution of the carboxylic acid by other functional groups, such as biotin,[33] boronic acid,[34] and organelle targeting motifs[35] known from the respective trackers,[36−38] has been recently achieved without a loss of function of the mechanophore. However, the targeting of organelles is neither uniform nor generally applicable to any membrane of interest (MOI). Namely, whereas well-established targeting units are available for lysosomes,[39,40] mitochondria,[41−43] and the endoplasmic reticulum (ER),[44] such units do not exist for many other subcellular compartments. To fluorescently image local tension in any MOI, we decided to develop a universally applicable targeting strategy based on self-labeling proteins (Figure 1A–C). These mutated enzymes can be easily expressed fused to a protein in the MOI inside living cells. Popular examples include the SNAP-tag,[45] CLIP-tag,[46] and HaloTag.[47,48] All of them present specific, orthogonal reactivity and fast kinetics with their corresponding benzylguanine, benzylcytosine, and chloroalkane ligands.[49,50]

Since the introduction of HaloTag technology,[48] the strategy has found many applications. Examples include protein labeling with synthetic ligands[48,51,52] or fluorescent dyes to study biological processes, such as redox signaling,[53,54] cell dynamics,[55−58] and protein degradation,[59] or to detect specific ions,[60−65] the viscosity,[22,66] and the membrane potential[18,23] inside compartments of living organisms. They were also used as covalent long-lived tethers for protein nanomechanics.[67−69] Moreover, several biological assays have been established in recent years that employ HaloTagging as the key step in their protocols,[70−72] including the chloroalkane penetration assay (CAPA)[73−75] for the quantification of cell permeability and cytosolic delivery. In this report, we explore the use of HaloTag technology for force imaging in mechanobiology. Exploiting the specificity of genetically encoded self-labeling enzymes, HaloFlippers are shown to target and report the membrane tension changes of various subcellular compartments, which were beyond the reach of traditional targeting units. These results introduce HaloFlippers as a universal tool to sense changes in the local tension and order in any MOI.

DESIGN AND SYNTHESIS OF HALOFLIPPERS

To localize flipper probes in the MOI using HaloTag technology, the flippers equipped with chloroalkane ligands

https://dx.doi.org/10.1021/acscentsci.0c00666
ACS Cent. Sci. 2020, 6, 1376−1385

and HaloTag proteins fused to the protein in the MOI are required (Figure 1A). The reaction between the ligand and a carboxylic acid in the engineered active site[48] should afford an ester that tethers the flipper to the fusion protein (Figure 1B). For operational flippers, the tether linking them to the membrane protein has to be loose enough to allow the insertion of the probe in the surrounding membrane (Figure 1, red). Moreover, the tether has to be hydrophilic enough to stay out of the membrane but lipophilic enough to diffuse passively across the plasma membrane.[23,59,63,76] We chose oligoethylene glycols of different lengths to identify the best tether: HaloFlippers **2**–**5** with a linear oligoethylene glycol containing 24, 16, 8, and 0 monomer repeats (Figure 1D). Control **6** is as tightly tethered as **5** but as hydrophilic as **3** with an ethylene glycol 16-mer. Flippers **2**–**6** were prepared following the procedures similar to those of **1** (Schemes S1–S4). Reflecting their higher hydrophilicity, flippers with longer tethers, **2** and **3**, were eluted at shorter retention times (R_t) from reverse-phase high-performance liquid chromatography (HPLC) compared with **4** and **5**, whereas R_t of **6** was similar to that of **4** (Figures S46–S50).

TETHER OPTIMIZATION

The relative partitioning efficiencies D_{rel} of flippers **2**–**5** were estimated in large unilamellar vesicles (LUVs) composed of solid-ordered (S_o) dipalmitoylphosphatidylcholine (DPPC) membranes (Table 1 and Figure S2). Flipper **2** with the longest tether showed poor retention in these artificial lipid bilayer membranes, whereas **4**–**6** inserted more efficiently into the membrane, and flipper **3** showed intermediate behavior. These results were consistent with their hydrophilicity estimated from R_t. The phase transition from liquid-disordered (L_d) to S_o membranes shifted the excitation maximum of flippers **2**–**6** to the red (Figure S2). As described in the Introduction, this red shift originated from planarization of the twisted push–pull probes in the ground state, thus confirming that the mechanosensitivity of flippers **2**–**6** needed to image membrane is intact.

Table 1. Characteristics of HaloFlipper Probes[a]

Cpd[b]	EC_{50} (nM)[c]	EC_{50}' (nM)[d]	D_{rel}[e]	r^2[f]	PCC[g]
2	34	17	0.23	0.96	0.93
3	89	25	0.39	0.94	0.93
4	4800	130	0.99	0.55	0.85
5	2900	240	1.00	0.35	0.87
6	3600	630	0.81	0.49	0.71

[a]Expanded version, with errors: Tables S2 and S3. [b]HaloFlipper probes. [c]Effective flipper concentration needed to label 50% of HaloTags on mitochondria in the cytosol of HGM cells after 15 min of incubation. Experiments were performed in duplicate. [d]Same for 45 min of incubation. [e]Relative partitioning efficiencies of the probes in solid-ordered membranes of DPPC LUVs, estimated from their fluorescence intensity. [f]Goodness of fit correlating flipper and GFP flourescence, extracted from the linear regression in Figure 2B and Figure S7. [g]Pearson correlation coefficient between the fluorescence signal from GFP and HaloFlippers, obtained from the manual analysis of five to six different cells/probe, as in Figure 2D and Figure S8.

The cellular permeabilities of HaloFlippers **2**–**6** were evaluated using the recently introduced CAPA,[73,74,77] adapted to high-content fluorescence microscopy (HC-CAPA, Figures S4–S6).[75] HC-CAPA uses HGM cells that are HeLa cells stably expressing a fusion protein of HaloTag and green fluorescent protein (GFP) on the outer surface of their mitochondria.[78] These cells were first treated with the HaloFlippers and then chased with a chloroalkylated rhodamine (HRO, Figure S1) that reacts and fluorescently labels all remaining free HaloTags. HC-CAPA provides rapid access to the dose–response curves and the EC_{50} of the respective substrate. According to EC_{50} = 34 ± 2 nM, HaloFlipper **2**, with the longest tether, entered the cytosol most efficiently (Figure 2A). With EC_{50} = 89 ± 14 nM, HaloFlipper **3** with a shorter tether closely followed. Further shortening of the tether significantly weakened the cellular uptake, degrading to 3–5 μM for **4**–**6**. Prolongated incubation times from 15 to 45 min resulted in lower EC_{50}' values, but the trend remained the same (Table 1, Figure S6, and Table S2).

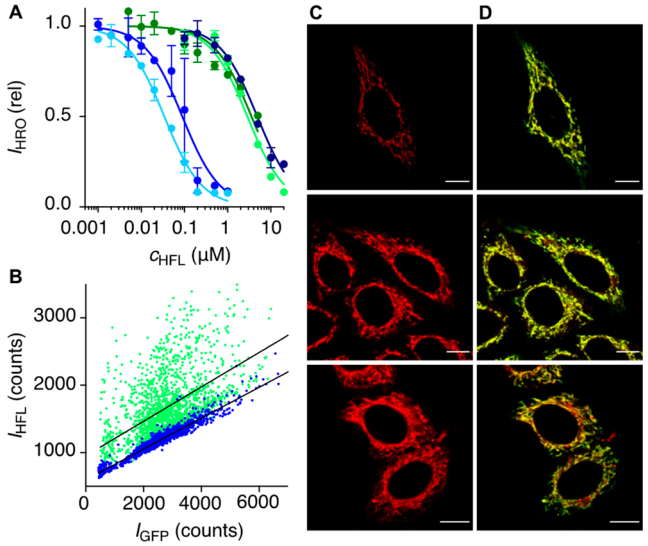

Figure 2. (A) HC-CAPA dose–response curves after 15 min of incubation of HGM cells with HaloFlippers (HFL) **2** (light blue), **3** (intense blue), **4** (dark blue), **5** (light green), and **6** (dark green). (B) Fluorescence intensity of GFP (proportional to HaloTag expression) versus fluorescence intensity of HFL **3** (intense blue) and **5** (light green) in the whole cells at their EC_{50}' with linear curve fit (1 dot = 1 cell). Data were automatically analyzed. (C) CLSM images of HGM cells after incubation with **2**–**4** (top down) at their EC_{50}. Laser power and postacquisition image treatment were kept constant. (D) As in panel C, merged images of HFL (red) and GFP (green). Brightness and contrast of the fluorescence of HaloFlippers were adjusted to comparable values. Scale bars: 10 μm. Experiments were performed in duplicate for panels A and B.

The cellular uptake of flippers **2**–**6** thus increased with decreasing partitioning. This indicated that entry into the membranes on one side is less important than release on the other side, thus implying that flippers that do not reach the cytosol end up trapped within membranes on the way. However, partitioning and uptake depended on the molecular architecture beyond the simple oligoethylene glycol length. Control **6** is as tightly tethered as **5** but contains an ethylene glycol 16-mer like **3** (Figure 1D). However, **6** showed similar partitioning and uptake properties to **5** rather than to **3**, presumably due to entropic reasons (Table 1, Figure 2A).[79–81]

The validity and significance of these conclusions were confirmed by comparing the fluorescence intensities of GFP and flippers **2**–**6** cell by cell. The large-scale analysis of statistically significant populations (>1000 analyzed cells per experiment) revealed perfect correlations with the efficiently

https://dx.doi.org/10.1021/acscentsci.0c00666
ACS Cent. Sci. 2020, 6, 1376–1385

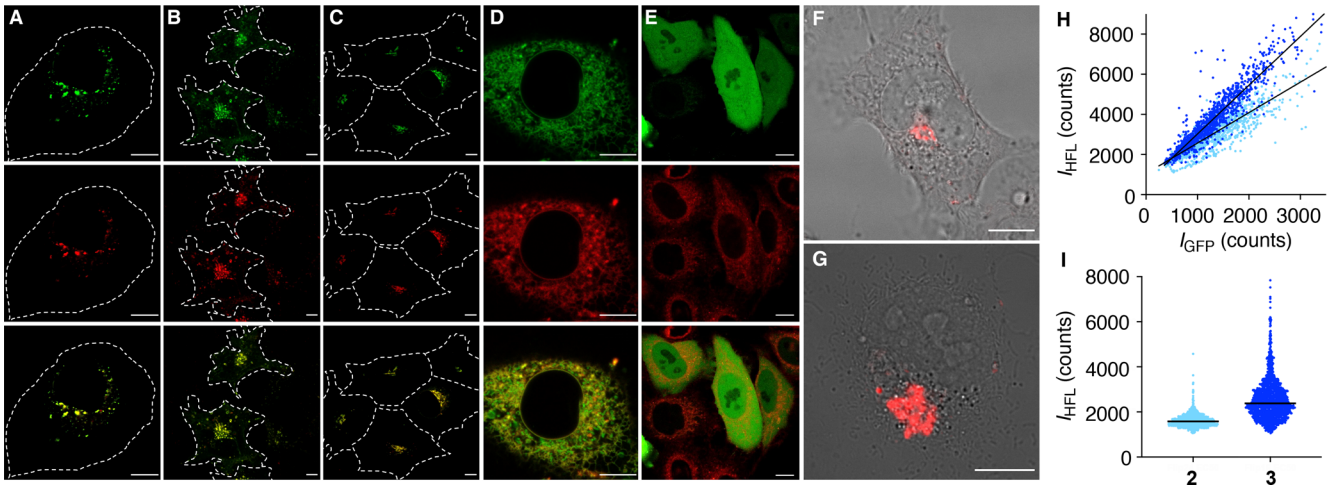

Figure 3. CLSM images of COS-7 cells expressing HaloTag and GFP on the membrane of (A) peroxisomes (PEX3-GFP-HaloTag, **p1**, Figure 4), (B) endolysosomes (LAMP1-HaloTag-GFP, **p2**), and (C) Golgi apparatus (GTS-HaloTag-GFP, **p3**) after incubation with **3** (90 nM, 15 min). Top: GFP; middle: **3**; bottom: merged. (D) CLSM images of COS-7 cells expressing HaloTag on the membrane of ER (HaloTag-Sec61B, **p6**) after coincubation with **3** (90 nM, 15 min) and ER-Tracker (1 μM, 15 min). Top: ER-Tracker; middle: **3**; bottom: merged. (E) CLSM images of HeLa Kyoto cells expressing HaloTag in the cytoplasm (**p10**) after incubation with **3** (1 μM, 15 min) followed by incubation with HRO (5 μM, 15 min). Top: HRO; middle: **3**; bottom: merged. (F) CLSM image of COS-7 cell expressing ManII-HaloTag fusion protein (Golgi apparatus, **p5**) after incubation with **3** (90 nM, 15 min). (G) Same as panel F, using HaloTag-ST as a fusion protein (**p4**, Golgi apparatus). (H) Fluorescence intensity of GFP (proportional to HaloTag expression) versus fluorescence intensity of **2** (17 nM, 45 min, light blue) and **3** (25 nM, 45 min, intense blue) in HeLa cells expressing GTS-HaloTag-GFP (**p3**, 1 dot = 1 cell) with linear curve fit. (I) Fluorescence intensity of **2** (17 nM, 45 min, light blue) and **3** (25 nM, 45 min, intense blue) in HeLa cells expressing cP450-HaloTag (**p7**, 1 dot = 1 cell) with straight lines corresponding to median values. Scale bars: 10 μm. Experiments were performed in duplicate for panels H and I.

penetrating flippers **2** and **3** (Figure 2B, Figure S7, Table 1, and Table S3, $r^2 > 0.93$). In clear contrast, flippers **4**–**6** showed poor correlation with GFP fluorescence ($r^2 < 0.56$). These results were consistent with the highly selective labeling of the HaloTag-GFP fusion protein by **2** and **3** and the less selective staining by **4**–**6**.

The analysis of the fluorescence microscopic images revealed identical trends (Figure 2C,D). The subcellular colocalizations of the fluorescence signals from GFP and flippers were quantified as Pearson correlation coefficients (PCCs). PCCs as high as 0.93 were extracted for the operational flippers **2** and **3**, whereas the rest exhibited more modest values, down to 0.71 for control **6** (Table 1, Figure S8). In confocal laser scanning microscopy (CLSM) images of HGM cells, flipper **3** was brighter than **2** (Figure 2C). Because flipper fluoresces only inside lipid bilayer membranes, this result suggested that the partitioning of the HaloTagged flipper **3** is better than that of **2**. This difference could be explained by the excess hydrophilicity added by the long tether in **2**, preventing partitioning,[63] or the too high entropy cost of the flipper insertion into the membrane due to the restricted rotations of the many single bonds in the longer tether.[79−81] In any case, the poor fluorescence of flipper **2** was inadequate for its use as a chemistry tool to image localized membrane tension changes in living cells. These results thus identified HaloFlipper **3** as the best among probes **2**–**6** for this purpose. The intermediate tether length of ∼6 nm (Figure S3) of the best HaloFlipper **3** revealed characteristic Goldilocks behavior,[75,82] offering the right balance of hydrophilicity and length needed for cell penetration and insertion into the MOI after reacting with the HaloTag.

SPECIFIC LABELING OF SUBCELLULAR MEMBRANES

The best HaloFlipper **3** was used together with the ultraloose analog **2** for the targeting of fusion proteins **p1**–**p10** in different subcellular compartments, including also MOIs that are beyond the reach of nonuniversal empirical tracking approaches (Figures 3 and 4). HaloTag- and GFP-fused

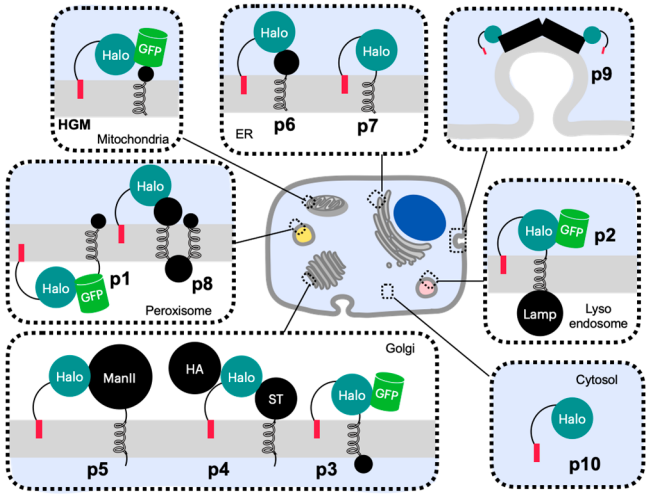

Figure 4. Schematic presentation of protein conjugates with HaloFlipper **3** used in this study. Flipper chromophores: red rectangles; HaloTags: teal filled circles; GFPs: green cylinders; other proteins: black. Protein sizes were roughly estimated from the number of amino acid residues. **p1**: PEX3-GFP-HaloTag, **p2**: LAMP1-HaloTag-meGFP, **p3**: GTS-HaloTag-meGFP, **p4**: ST-HaloTag-HA, **p5**: ManII-HaloTag, **p6**: HaloTag-Sec61B, **p7**: cP450-(C21)-HaloTag, **p8**: $HsPex3p_{(1-230)}$-HaloTag, **p9**: HaloTag-CLC, **p10**: free HaloTag (Table S1).

https://dx.doi.org/10.1021/acscentsci.0c00666
ACS Cent. Sci. 2020, 6, 1376−1385

membrane proteins in peroxisomes (PEX3, **p1**, Figure 3A and Figure S13A)[83] endolysosomes (LAMP1, **p2**, Figure 3B and Figure S13B),[49] and the Golgi apparatus (Golgi targeting sequence (GTS), **p3**, Figure 3C and Figures S3 and S13C),[49] were examined first. The fusion proteins were expressed by transient transfection of the cells with the corresponding plasmids. For all three systems, the colocalization of GFP with HaloFlippers **2** and **3** was excellent (Figure 3A−C). The flipper selectivity for the MOI was quantified with PCCs. PCC = 0.81, 0.88, and 0.94 were obtained for **3** targeting PEX3 (**p1**), LAMP1 (**p2**), and GTS (**p3**), respectively. This high selectivity obtained from the manual PCC analysis was supported by the automated image-based large-scale high-content analysis, which showed, again, good correlations between the fluorescence intensities of GFPs and flippers (Figure 3H and Figures S10−S12). The automated high-content analysis further confirmed that, as with the above HGM cells, the fluorescence intensity of **3** in the specific subcellular MOIs with the overexpressed proteins is generally higher compared with **2** (Figure 3H and Figures S10−S12). The Golgi apparatus was also targeted using resident proteins, including mannosidase II (ManII) and sialyltransferase (ST),[50] both with the self-labeling HaloTag fused to the lumen side of the proteins (Figures 3F,G and 4, **p4**, **p5**).[84,85]

Other fusion proteins from different organelles were also tested, including the minimal membrane anchoring domains of cytochrome P450 (cP450) and Sec61B,[86] both in the membrane of the ER, fused to the HaloTag on their cytosolic sides (Figure 3D; Figure 4, **p6**, **p7**; Figure S14). Lacking a fluorescence protein that would report on the expression level after transfection, we confirmed the selectivity of the HaloFlippers for the location of the corresponding MOIs with an ER-selective dye. Once again, the fluorescence intensity of **3** was higher than that of **2** in both cases (Figure 3I and Figure S12). Extra fusion proteins for peroxisomes[87] were examined as well, with equally good results (HsPex3p$_{(1-230)}$-HaloTag **p8**, Figure 4 and Figure S15).

Flipper emission from nontransfected cells was negligible (Figure S9). This general observation confirmed that the cellular uptake is reversible and the covalent capture by the fusion proteins is very efficient. Negligible off-target emission from nontransfected cells, at reasonable transfection levels, was important to exclude interference with membrane tension measurements in the MOI.

These results from different fusion proteins in different organelles confirmed HaloFlipper **3** as the best, with an intermediate 16-mer tether length of ∼ 6 nm offering the right hydrophilicity and length for efficient cell penetration and insertion into the MOI after reacting with the HaloTag (Figures 1 and 4 and Figure S3). The consistent trends supported that this conclusion is general, except for very large protein complexes where the HaloTag is expressed far from the MOI. In fact, images of HeLa cells with the clathrin coat overexpressed with the HaloTag fused to one of the light chains[50,88] did not show any substantial fluorescence signal after incubation with flipper **3** or **2** (HaloTag-CLC **p9**, Figure 4 and Figure S3 and S16). In contrast, CLSM images after treatment with the environment-insensitive HRO control[50] exhibited cells with fluorescence located in vesicular domains distributed in the cytoplasmic matrix, ruling out transfection efficiency issues (Figure S16). This result confirmed that HaloFlippers are silent outside the MOI; that is, they do not produce false positives with regard to the localized fluorescence imaging of membrane tension.

Further support for this important conclusion was obtained from HaloTags expressed freely in the cytosol (**p10**, Figure 4).[22] HaloTags colabeled using flipper **3** and HRO controls produced images with a homogeneous distribution of the fluorescence from the latter in the cytosol and nucleus. In contrast, the HaloFlipper emitted only weakly from organelle-like structures, even at concentrations far above the EC_{50} (1 μM instead of 90 nM, Figure 3E and Figure S17). Whether this fluorescence originated from HaloTag complexes with the hydrophobic flippers anchored in the subcellular membranes or from unreacted probes was not further important. The important point was the experimental confirmation that flippers bound to HaloTags do not emit from the media; that is, they do not interfere with the localized fluorescence imaging of membrane tension.

IMAGING CHANGES IN PHYSICAL PROPERTIES AND MEMBRANE TENSION

The compatibility of HaloFlipper **3** to fluorescently image tension applied to any MOI within living cells was explored with FLIM. The lifetime of HaloFlipper **3** in the ER, after incubation with cells transfected with the corresponding plasmids, was $\tau \approx 3.5$ ns (**p6**, **p7**, Figures 4 and 5A,E and Figure S18). The probe responded to a decrease in the membrane tension caused by hyperosmotic stress with a decrease in the fluorescence lifetime by $\Delta\tau \approx 0.3$ ns. These lifetimes and decreases were similar to changes found with flippers that target ER with the empirical, nonuniversal methods of ER trackers.[35] This similarity supported the notion that neither flipper−protein interactions nor the local environment influences the tension imaging by HaloFlipper **3**. In other words, the tether in **3** is long enough to allow sufficient diffusion of the flipper in membranes to report an average membrane tension change without interference from the protein.

Because of the transfection inefficiency of HsPex3p$_{(1-230)}$-HaloTag (**p8**) in COS-7 cells, peroxisome tension experiments were performed in HeLa Kyoto cells. The similar lifetime characteristics of peroxisomal and ER membrane, including their response to changes in the membrane tension (Figure 5E and Figure S20), were consistent with the notion that peroxisomes can form and gain their lipids from the ER membranes.[89,90]

The membrane of the Golgi apparatus, richer in cholesterol and sphingolipids,[91−93] revealed a higher order than the ER, with significant differences depending on the fusion protein. For instance, the lifetime of flipper **3** tagged to mannosidase II (**p5**, $\tau \approx 4.0$ ns) was higher than the one from sialyltransferase (**p4**, $\tau \approx 3.7$ ns, Figure 5). However, their responses to membrane tension applied by extracellular hyperosmotic stress were identical (Figure 5B,E and Figure S19). Like in the ER, this uniform response supported the notion that flipper probes report on the average tension changes in the MOI. Differences in absolute values indicated that flipper probes can also inform on the nature of the local membrane environment of the fusion protein. However, it is far from certain to assume that this will be the case with other constructs and expression levels.

To further elaborate on these conclusions, ManII-HaloTag (**p5**)-transfected cells were incubated for 15 h with 1.5 μM myriocin, a well-known antibiotic that inhibits sphingosine biosynthesis.[94] A control group of cells was treated with

https://dx.doi.org/10.1021/acscentsci.0c00666
ACS Cent. Sci. 2020, 6, 1376−1385

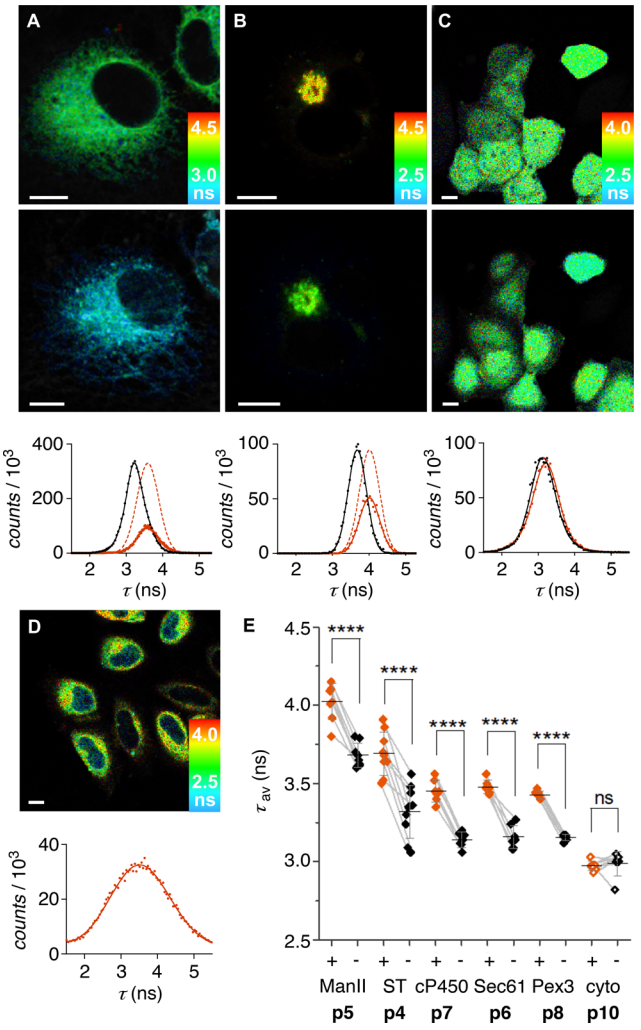

Figure 5. (A–C) FLIM images of cells expressing (A) cP450-HaloTag (**p7**), (B) ManII-HaloTag (**p5**), and (C) free HaloTag in cytosol (**p10**) labeled with **3** ((A,B) 90 nM, 15 min) or HRO ((C) 5 μM, 15 min) under isotonic (top) or hypertonic (middle) conditions with their corresponding lifetime histograms (bottom: red, isotonic; black, hypertonic; red dashed line, isotonic signal normalized to values of hypertonic). (D) FLIM image of cells expressing free HaloTag in cytosol (**p10**) labeled with **3** (90 nM, 15 min, top) and its corresponding lifetime histogram (bottom). Scale bars: 10 μm. (E) Fluorescence lifetimes of cells expressing ManII-HaloTag (**p5**), ST-HaloTag (**p4**), cP450-HaloTag (**p7**), HaloTag-Sec61 (**p6**), and HsPex3p$_{(1-230)}$-HaloTag (**p8**) labeled with **3** (90 nM, 15 min, filled diamonds) and free HaloTag (**p10**) labeled with HRO (5 μM, 15 min, empty diamonds) under isotonic (red) or hypertonic (black) conditions; 1 diamond = 1 measurement, with the solid black line corresponding to mean values, whiskers corresponding to the standard deviation, and the solid gray line matching measurements on the same cell. Statistical significance was determined using the one-tailed paired Student's t test: ns: $p > 0.05$, ****: $p < 0.0001$.

methanol only as a negative control under otherwise identical conditions. Both groups were stained with flipper **3**, visualized with FLIM, and subjected to osmotic shock (Figure 6A,B). Whereas the control group showed an almost identical lifetime and response to osmotic shock as discussed before (4.00–3.66 vs 4.02–3.68 ns), the sphingolipid depleted cells resulted in a clearly reduced lifetime (3.84 ns), suggesting that the lipid order indeed decreased (Figure 6C, Table S4). The response to osmotic shock remained comparable, indicating the

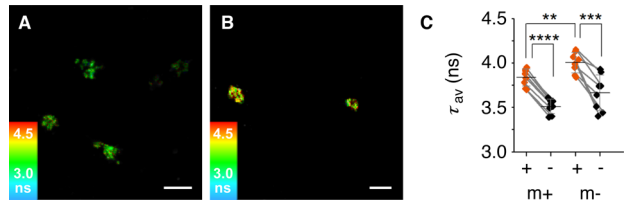

Figure 6. (A,B) FLIM images of cells expressing ManII-HaloTag (**p5**) treated with 1.5 μM myriocin (A) or methanol control (B) labeled with **3** (90 nM, 15 min). Scale bars: 10 μm. (C) Fluorescence lifetimes of cells from conditions A (m+) and B (m−) under isotonic (red) or hypertonic (black) conditions, with the one-tailed unpaired (m+ vs m−) or paired (+ vs −) Student's t test for comparing myriocin-treated cells with the control group for responses to osmotic shock: **: $p < 0.01$, ***: $p < 0.001$, ****: $p < 0.0001$.

continuing presence of sufficiently ordered domains for disassembly in response to the decreasing membrane tension ($\Delta\tau$ = 0.33 vs 0.34 ns).

These results nicely illustrated how to interpret flipper lifetimes in general: (i) Absolute lifetimes report on the overall physical properties of the MOI, increasing with order.[5,7] (ii) Lifetime changes can report on the membrane tension change, with lifetimes increasing with tension.[5,35]

For the experiment under discussion, the observed lower absolute lifetimes upon sphingolipid depletion are consistent with reduced membrane order (Figure 6A,B). For the preceding experiment giving different lifetimes for different fusion proteins in the same organelle, this could imply that the membrane environments around the two fusion proteins differ, and flipper probes inform on their order (**p4** vs **p5** but not **p6** vs **p7**, Figures 4 and 5E). However, the decreases in lifetimes under osmotic stress were uniform in both cases (Figures 5E and 6C). Thus membrane tension imaging is operational, independent of the composition of the MOI. Lifetimes are independent of transfection efficiency as long as off-target effects from overtransfection can be excluded; such problems are, however, general and unrelated to flipper probes.

FLIM images of HaloTags freely expressed in the cytoplasm were recorded as negative controls. The reaction with the environment-insensitive HRO control produced homogeneous fluorescence throughout the cytosol and nucleus, as already described (Figure 3E). Osmotic stress applied to these cells did not change the fluorescence lifetimes (Figure 5C,E). In contrast, cytosolic HaloTags reacted with flipper **3** produced a very heterogeneous distribution of lifetimes, reflecting the location in different subcellular membranes of different composition. The full width at half-maximum (fwhm) of the lifetime histogram was $w \approx 2.0$ ns, more than twice as large as the fwhm of the lifetime histogram from flippers in ER ($w \approx 0.7$ ns) or Golgi ($w \approx 0.6$ ns, Figure 5D vs Figure 5A,B). This fwhm broadening obtained with nonlocalized flipper probes confirmed that the localization of flipper probes in a specific MOI is ultimately essential for the meaningful and tractable fluorescence imaging of membrane tension within living cells.

CONCLUSIONS

Small-molecule chemistry tools to fluorescently image physical forces will be needed to tackle mechanobiology. We have previously introduced flipper probes to image membrane tension changes in living cells with FLIM. Here we introduce HaloFlippers to specifically localize fluorescent tension probes to any MOI. This is achieved by first expressing HaloTag

https://dx.doi.org/10.1021/acscentsci.0c00666
ACS Cent. Sci. 2020, 6, 1376–1385

fusion proteins on that MOI. These HaloTags then react with fluorescent force probes equipped with a chloroalkane at the end of a long enough (but not too long) tether, that is, HaloFlippers.

With the best HaloFlipper, we demonstrate that the targeting of MOIs is general in the broadest sense. Important examples include organelles (e.g., Golgi, peroxisomes) that are not easily targeted with the nonuniversal, empirical methods known from the respective trackers (mitochondria, ER, endolysosomes).

Upon installation, HaloFlippers report on the nature of the MOI, with lifetimes increasing with membrane order. For example, the lifetimes in the more ordered Golgi membranes (up to $\tau \approx 4.1$ ns) clearly exceed those of the ER (up to $\tau \approx 3.5$ ns). Changing the composition of the MOI, that is, sphingomyelin depletion in the Golgi, shortens lifetimes, as expected for decreasing order ($\tau \approx 4.02-3.84$ ns), whereas the responsiveness to membrane tension remains intact.

Increasing tension applied to the MOI by osmotic stress is reported as an increase in lifetime, and decreasing tension is reported as a decreasing lifetime. The magnitude of the response to tension does not depend much on the nature of the MOI. Examples reach from $\Delta\tau = 0.37$ to 0.27 ns for the same level of osmotic stress. HaloFlippers localized in MOIs yield a high resolution, characterized by the fwhm of the lifetime histogram around $w \approx 0.7$ ns. Controls with targetless flippers contrast with $w \approx 2.0$ ns. This important difference demonstrates that precise probe localization in the MOI is ultimately unavoidable for significant tension imaging in living cells.

HaloTagged control dyes without mechanosensitivity do not change the lifetime in response to tension changes ($\Delta\tau = -0.02$ ns for rhodamines). Controls further confirm that HaloTagged flippers that cannot insert into membranes do not fluoresce. For instance, loading of a HaloTag expressed in the cytosol produces bright diffuse fluorescence with rhodamines but not with flippers. These results demonstrate that HaloFlippers are ready for use in mechanobiology in the broadest sense. The response from the community to the original Flipper-TR operating on the surface of cells suggests that a chemistry tool to image membrane tension exclusively in MOIs everywhere within cells will satisfy an important and urgent need.

■ ASSOCIATED CONTENT

Supporting Information

The Supporting Information is available free of charge at https://pubs.acs.org/doi/10.1021/acscentsci.0c00666.

Materials and methods, synthesis of HaloFlippers, comparison of HaloFlippers in LUVs, cell lines and plasmids, comparison of HaloFlippers in cells, MOI scope of HaloFlippers, fluorescence lifetimes, supporting references, NMR spectra, and LCMS traces of final compounds (PDF)

■ AUTHOR INFORMATION

Corresponding Authors

Stefan Matile − *School of Chemistry and Biochemistry and National Centre of Competence in Research (NCCR) Chemical Biology, University of Geneva, Geneva 1211, Switzerland*; orcid.org/0000-0002-8537-8349; Email: stefan.matile@unige.ch

Javier López-Andarias − *School of Chemistry and Biochemistry and National Centre of Competence in Research (NCCR) Chemical Biology, University of Geneva, Geneva 1211, Switzerland*; Email: javier.lopez@unige.ch

Authors

Karolína Straková − *School of Chemistry and Biochemistry and National Centre of Competence in Research (NCCR) Chemical Biology, University of Geneva, Geneva 1211, Switzerland*

Noemi Jiménez-Rojo − *School of Chemistry and Biochemistry and National Centre of Competence in Research (NCCR) Chemical Biology, University of Geneva, Geneva 1211, Switzerland*

Joseph E. Chambers − *Cambridge Institute for Medical Research, University of Cambridge, Cambridge CB2 0XY, United Kingdom*; orcid.org/0000-0003-4675-0053

Stefan J. Marciniak − *Cambridge Institute for Medical Research, University of Cambridge, Cambridge CB2 0XY, United Kingdom*; orcid.org/0000-0001-8472-7183

Howard Riezman − *School of Chemistry and Biochemistry and National Centre of Competence in Research (NCCR) Chemical Biology, University of Geneva, Geneva 1211, Switzerland*; orcid.org/0000-0003-4680-9422

Naomi Sakai − *School of Chemistry and Biochemistry and National Centre of Competence in Research (NCCR) Chemical Biology, University of Geneva, Geneva 1211, Switzerland*

Complete contact information is available at: https://pubs.acs.org/10.1021/acscentsci.0c00666

Author Contributions

[§]K.S. and J.L.-A. contributed equally to this study.

Notes

The authors declare the following competing financial interest(s): The University of Geneva has licensed Flipper-TR to Spirochrome for commercialization.

■ ACKNOWLEDGMENTS

We thank D. Moreau and S. Vossio for the help with the high-content microscopy and analysis, V. Mercier, A. Colom, and C. Roffay for the help with the FLIM, J. A. Kritzer (Tufts University), M. Fransen (Leuven University), C. Blackstone (NIH, Bethesda), D. Toomre (Yale University), M. Hensel (Osnabrück University), and M. A. Lampson (University of Pennsylvania) for providing materials (details in Table S1), the NMR, the MS, and the Bioimaging and ACCESS platforms for services, and the University of Geneva, the National Centre Chemical Biology (NCCR) Chemical Biology, the NCCR Molecular Systems Engineering, and the Swiss NSF for financial support.

■ REFERENCES

(1) Leiphart, R. J.; Chen, D.; Peredo, A. P.; Loneker, A. E.; Janmey, P. A. Mechanosensing at Cellular Interfaces. *Langmuir* **2019**, *35*, 7509−7519.

(2) Pontes, B.; Monzo, P.; Gauthier, N. C. Membrane Tension: A Challenging but Universal Physical Parameter in Cell Biology. *Semin. Cell Dev. Biol.* **2017**, *71*, 30−41.

(3) Roca-Cusachs, P.; Conte, V.; Trepat, X. Quantifying Forces in Cell Biology. *Nat. Cell Biol.* **2017**, *19*, 742−751.

(4) Krieg, M.; Fläschner, G.; Alsteens, D.; Gaub, B. M.; Roos, W. H.; Wuite, G. J. L.; Gaub, H. E.; Gerber, C.; Dufrêne, Y. F.; Müller, D. J. Atomic Force Microscopy-Based Mechanobiology. *Nat. Rev. Phys.* **2019**, *1*, 41−57.

(5) Colom, A.; Derivery, E.; Soleimanpour, S.; Tomba, C.; Molin, M. D.; Sakai, N.; González-Gaitán, M.; Matile, S.; Roux, A. A Fluorescent Membrane Tension Probe. *Nat. Chem.* **2018**, *10*, 1118−1125.
(6) Strakova, K.; Poblador-Bahamonde, A. I.; Sakai, N.; Matile, S. Fluorescent Flipper Probes: Comprehensive Twist Coverage. *Chem. - Eur. J.* **2019**, *25*, 14935−14942.
(7) Dal Molin, M.; Verolet, Q.; Colom, A.; Letrun, R.; Derivery, E.; Gonzalez-Gaitan, M.; Vauthey, E.; Roux, A.; Sakai, N.; Matile, S. Fluorescent Flippers for Mechanosensitive Membrane Probes. *J. Am. Chem. Soc.* **2015**, *137*, 568−571.
(8) Soleimanpour, S.; Colom, A.; Derivery, E.; Gonzalez-Gaitan, M.; Roux, A.; Sakai, N.; Matile, S. Headgroup Engineering in Mechanosensitive Membrane Probes. *Chem. Commun.* **2016**, *52*, 14450−14453.
(9) Riggi, M.; Bourgoint, C.; Macchione, M.; Matile, S.; Loewith, R.; Roux, A. TORC2 Controls Endocytosis through Plasma Membrane Tension. *J. Cell Biol.* **2019**, *218*, 2265−2276.
(10) Riggi, M.; Niewola-Staszkowska, K.; Chiaruttini, N.; Colom, A.; Kusmider, B.; Mercier, V.; Soleimanpour, S.; Stahl, M.; Matile, S.; Roux, A.; Loewith, R. Decrease in Plasma Membrane Tension Triggers PtdIns(4,5)P2 Phase Separation to Inactivate TORC2. *Nat. Cell Biol.* **2018**, *20*, 1043−1051.
(11) Strakova, K.; Assies, L.; Goujon, A.; Piazzolla, F.; Humeniuk, H. V.; Matile, S. Dithienothiophenes at Work: Access to Mechanosensitive Fluorescent Probes, Chalcogen-Bonding Catalysis, and Beyond. *Chem. Rev.* **2019**, *119*, 10977−11005.
(12) Cinar, M. E.; Ozturk, T. Thienothiophenes, Dithienothiophenes, and Thienoacenes: Syntheses, Oligomers, Polymers, and Properties. *Chem. Rev.* **2015**, *115*, 3036−3140.
(13) Macchione, M.; Goujon, A.; Strakova, K.; Humeniuk, H. V.; Licari, G.; Tajkhorshid, E.; Sakai, N.; Matile, S. A Chalcogen-Bonding Cascade Switch for Planarizable Push−Pull Probes. *Angew. Chem., Int. Ed.* **2019**, *58*, 15752−15756.
(14) Bauzá, A.; Mooibroek, T. J.; Frontera, A. The Bright Future of Unconventional σ/π-Hole Interactions. *ChemPhysChem* **2015**, *16*, 2496−2517.
(15) Begum, S.; Cianci, M.; Durbeej, B.; Falklöf, O.; Hädener, A.; Helliwell, J. R.; Helliwell, M.; Regan, A. C.; Watt, C. I. F. On the Origin and Variation of Colors in Lobster Carapace. *Phys. Chem. Chem. Phys.* **2015**, *17*, 16723−16732.
(16) Gamiz-Hernandez, A. P.; Angelova, I. N.; Send, R.; Sundholm, D.; Kaila, V. R. I. Protein-Induced Color Shift of Carotenoids in β-Crustacyanin. *Angew. Chem., Int. Ed.* **2015**, *54*, 11564−11566.
(17) Baumeister, B.; Matile, S. Rigid-Rod β-Barrels as Lipocalin Models: Probing Confined Space by Carotenoid Encapsulation. *Chem. - Eur. J.* **2000**, *6*, 1739−1749.
(18) Abdelfattah, A. S.; Kawashima, T.; Singh, A.; Novak, O.; Liu, H.; Shuai, Y.; Huang, Y.-C.; Campagnola, L.; Seeman, S. C.; Yu, J.; Zheng, J.; Grimm, J. B.; Patel, R.; Friedrich, J.; Mensh, B. D.; Paninski, L.; Macklin, J. J.; Murphy, G. J.; Podgorski, K.; Lin, B.-J.; Chen, T.-W.; Turner, G. C.; Liu, Z.; Koyama, M.; Svoboda, K.; Ahrens, M. B.; Lavis, L. D.; Schreiter, E. R. Bright and Photostable Chemigenetic Indicators for Extended in Vivo Voltage Imaging. *Science* **2019**, *365*, 699−704.
(19) Kiser, P. D.; Golczak, M.; Palczewski, K. Chemistry of the Retinoid (Visual) Cycle. *Chem. Rev.* **2014**, *114*, 194−232.
(20) Sheves, M.; Nakanishi, N.; Honig, B. Through-Space Electrostatic Effects in Electronic Spectra. Experimental Evidence for the External Point-Charge Model of Visual Pigments. *J. Am. Chem. Soc.* **1979**, *101*, 7086−7088.
(21) Klymchenko, A. S. Solvatochromic and Fluorogenic Dyes as Environment-Sensitive Probes: Design and Biological Applications. *Acc. Chem. Res.* **2017**, *50*, 366−375.
(22) Chambers, J. E.; Kubánková, M.; Huber, R. G.; López-Duarte, I.; Avezov, E.; Bond, P. J.; Marciniak, S. J.; Kuimova, M. K. An Optical Technique for Mapping Microviscosity Dynamics in Cellular Organelles. *ACS Nano* **2018**, *12*, 4398−4407.
(23) Deal, P. E.; Liu, P.; Al-Abdullatif, S. H.; Muller, V. R.; Shamardani, K.; Adesnik, H.; Miller, E. W. Covalently Tethered Rhodamine Voltage Reporters for High Speed Functional Imaging in Brain Tissue. *J. Am. Chem. Soc.* **2020**, *142*, 614−622.
(24) Xiong, Y.; Vargas Jentzsch, A.; Osterrieth, J. W. M.; Sezgin, E.; Sazanovich, I. V.; Reglinski, K.; Galiani, S.; Parker, A. W.; Eggeling, C.; Anderson, H. L. Spironaphthoxazine Switchable Dyes for Biological Imaging. *Chem. Sci.* **2018**, *9*, 3029−3040.
(25) Humeniuk, H. V.; Rosspeintner, A.; Licari, G.; Kilin, V.; Bonacina, L.; Vauthey, E.; Sakai, N.; Matile, S. White-Fluorescent Dual-Emission Mechanosensitive Membrane Probes That Function by Bending Rather than Twisting. *Angew. Chem., Int. Ed.* **2018**, *57*, 10559−10563.
(26) Muraoka, T.; Umetsu, K.; Tabata, K. V.; Hamada, T.; Noji, H.; Yamashita, T.; Kinbara, K. Mechano-Sensitive Synthetic Ion Channels. *J. Am. Chem. Soc.* **2017**, *139*, 18016−18023.
(27) Haidekker, M. A.; Theodorakis, E. A. Ratiometric Mechanosensitive Fluorescent Dyes: Design and Applications. *J. Mater. Chem. C* **2016**, *4*, 2707−2718.
(28) Niko, Y.; Didier, P.; Mely, Y.; Konishi, G.; Klymchenko, A. S. Bright and Photostable Push-Pull Pyrene Dye Visualizes Lipid Order Variation between Plasma and Intracellular Membranes. *Sci. Rep.* **2016**, *6*, 18870.
(29) Ho, J. C. S.; Rangamani, P.; Liedberg, B.; Parikh, A. N. Mixing Water, Transducing Energy, and Shaping Membranes: Autonomously Self-Regulating Giant Vesicles. *Langmuir* **2016**, *32*, 2151−2163.
(30) Uline, M. J.; Schick, M.; Szleifer, I. Phase Behavior of Lipid Bilayers under Tension. *Biophys. J.* **2012**, *102*, 517−522.
(31) Chen, D.; Santore, M. M. Three Dimensional (Temperature−Tension−Composition) Phase Map of Mixed DOPC−DPPC Vesicles: Two Solid Phases and a Fluid Phase Coexist on Three Intersecting Planes. *Biochim. Biophys. Acta, Biomembr.* **2014**, *1838*, 2788−2797.
(32) Baumgart, T.; Hess, S. T.; Webb, W. W. Imaging Coexisting Fluid Domains in Biomembrane Models Coupling Curvature and Line Tension. *Nature* **2003**, *425*, 821−824.
(33) Goujon, A.; Straková, K.; Sakai, N.; Matile, S. Streptavidin Interfacing as a General Strategy to Localize Fluorescent Membrane Tension Probes in Cells. *Chem. Sci.* **2019**, *10*, 310−319.
(34) Strakova, K.; Soleimanpour, S.; Diez-Castellnou, M.; Sakai, N.; Matile, S. Ganglioside-Selective Mechanosensitive Fluorescent Membrane Probes. *Helv. Chim. Acta* **2018**, *101*, e1800019.
(35) Goujon, A.; Colom, A.; Straková, K.; Mercier, V.; Mahecic, D.; Manley, S.; Sakai, N.; Roux, A.; Matile, S. Mechanosensitive Fluorescent Probes to Image Membrane Tension in Mitochondria, Endoplasmic Reticulum, and Lysosomes. *J. Am. Chem. Soc.* **2019**, *141*, 3380−3384.
(36) Wagner, N.; Stephan, M.; Höglinger, D.; Nadler, A. A Click Cage: Organelle-Specific Uncaging of Lipid Messengers. *Angew. Chem., Int. Ed.* **2018**, *57*, 13339−13343.
(37) Xu, W.; Zeng, Z.; Jiang, J.-H.; Chang, Y.-T.; Yuan, L. Discerning the Chemistry in Individual Organelles with Small-Molecule Fluorescent Probes. *Angew. Chem., Int. Ed.* **2016**, *55*, 13658−13699.
(38) Zhu, H.; Fan, J.; Du, J.; Peng, X. Fluorescent Probes for Sensing and Imaging within Specific Cellular Organelles. *Acc. Chem. Res.* **2016**, *49*, 2115−2126.
(39) Wallabregue, A.; Moreau, D.; Sherin, P.; Moneva Lorente, P.; Jarolímová, Z.; Bakker, E.; Vauthey, E.; Gruenberg, J.; Lacour, J. Selective Imaging of Late Endosomes with a pH-Sensitive Diazaoxatriangulene Fluorescent Probe. *J. Am. Chem. Soc.* **2016**, *138*, 1752−1755.
(40) Takahashi, S.; Kagami, Y.; Hanaoka, K.; Terai, T.; Komatsu, T.; Ueno, T.; Uchiyama, M.; Koyama-Honda, I.; Mizushima, N.; Taguchi, T.; Arai, H.; Nagano, T.; Urano, Y. Development of a Series of Practical Fluorescent Chemical Tools To Measure pH Values in Living Samples. *J. Am. Chem. Soc.* **2018**, *140*, 5925−5933.
(41) Jiménez-Sánchez, A.; Lei, E. K.; Kelley, S. O. A Multifunctional Chemical Probe for the Measurement of Local Micropolarity and

Microviscosity in Mitochondria. *Angew. Chem., Int. Ed.* **2018**, *57*, 8891−8895.
(42) Yang, Z.; He, Y.; Lee, J.-H.; Park, N.; Suh, M.; Chae, W.-S.; Cao, J.; Peng, X.; Jung, H.; Kang, C.; Kim, J. S. A Self-Calibrating Bipartite Viscosity Sensor for Mitochondria. *J. Am. Chem. Soc.* **2013**, *135*, 9181−9185.
(43) Feng, S.; Harayama, T.; Montessuit, S.; David, F. P.; Winssinger, N.; Martinou, J.-C.; Riezman, H. Mitochondria-Specific Photoactivation to Monitor Local Sphingosine Metabolism and Function. *eLife* **2018**, *7*, e34555.
(44) Meinig, J. M.; Fu, L.; Peterson, B. R. Synthesis of Fluorophores That Target Small Molecules to the Endoplasmic Reticulum of Living Mammalian Cells. *Angew. Chem., Int. Ed.* **2015**, *54*, 9696−9699.
(45) Keppler, A.; Gendreizig, S.; Gronemeyer, T.; Pick, H.; Vogel, H.; Johnsson, K. A General Method for the Covalent Labeling of Fusion Proteins with Small Molecules in Vivo. *Nat. Biotechnol.* **2003**, *21*, 86−89.
(46) Gautier, A.; Juillerat, A.; Heinis, C.; Corrêa, I. R.; Kindermann, M.; Beaufils, F.; Johnsson, K. An Engineered Protein Tag for Multiprotein Labeling in Living Cells. *Chem. Biol.* **2008**, *15*, 128−136.
(47) England, C. G.; Luo, H.; Cai, W. HaloTag Technology: A Versatile Platform for Biomedical Applications. *Bioconjugate Chem.* **2015**, *26*, 975−986.
(48) Los, G. V.; Encell, L. P.; McDougall, M. G.; Hartzell, D. D.; Karassina, N.; Zimprich, C.; Wood, M. G.; Learish, R.; Ohana, R. F.; Urh, M.; Simpson, D.; Mendez, J.; Zimmerman, K.; Otto, P.; Vidugiris, G.; Zhu, J.; Darzins, A.; Klaubert, D. H.; Bulleit, R. F.; Wood, K. V. HaloTag: A Novel Protein Labeling Technology for Cell Imaging and Protein Analysis. *ACS Chem. Biol.* **2008**, *3*, 373−382.
(49) Liss, V.; Barlag, B.; Nietschke, M.; Hensel, M. Self-Labelling Enzymes as Universal Tags for Fluorescence Microscopy, Super-Resolution Microscopy and Electron Microscopy. *Sci. Rep.* **2016**, *5*, 17740.
(50) Erdmann, R. S.; Baguley, S. W.; Richens, J. H.; Wissner, R. F.; Xi, Z.; Allgeyer, E. S.; Zhong, S.; Thompson, A. D.; Lowe, N.; Butler, R.; Bewersdorf, J.; Rothman, J. E.; St Johnston, D.; Schepartz, A.; Toomre, D. Labeling Strategies Matter for Super-Resolution Microscopy: A Comparison between HaloTags and SNAP-Tags. *Cell Chem. Biol.* **2019**, *26*, 584−592.
(51) Frei, M. S.; Hoess, P.; Lampe, M.; Nijmeijer, B.; Kueblbeck, M.; Ellenberg, J.; Wadepohl, H.; Ries, J.; Pitsch, S.; Reymond, L.; Johnsson, K. Photoactivation of Silicon Rhodamines via a Light-Induced Protonation. *Nat. Commun.* **2019**, *10*, 4580.
(52) Murrey, H. E.; Judkins, J. C.; am Ende, C. W.; Ballard, T. E.; Fang, Y.; Riccardi, K.; Di, L.; Guilmette, E. R.; Schwartz, J. W.; Fox, J. M.; Johnson, D. S. Systematic Evaluation of Bioorthogonal Reactions in Live Cells with Clickable HaloTag Ligands: Implications for Intracellular Imaging. *J. Am. Chem. Soc.* **2015**, *137*, 11461−11475.
(53) Parvez, S.; Long, M. J. C.; Poganik, J. R.; Aye, Y. Redox Signaling by Reactive Electrophiles and Oxidants. *Chem. Rev.* **2018**, *118*, 8798−8888.
(54) Parvez, S.; Long, M. J. C.; Lin, H.-Y.; Zhao, Y.; Haegele, J. A.; Pham, V. N.; Lee, D. K.; Aye, Y. T-REX on-Demand Redox Targeting in Live Cells. *Nat. Protoc.* **2016**, *11*, 2328−2356.
(55) Jonker, C. T. H.; Deo, C.; Zager, P. J.; Tkachuk, A. N.; Weinstein, A. M.; Rodriguez-Boulan, E.; Lavis, L. D.; Schreiner, R. Accurate Measurement of Fast Endocytic Recycling Kinetics in Real Time. *J. Cell Sci.* **2020**, *133*, jcs231225.
(56) Asanuma, D.; Takaoka, Y.; Namiki, S.; Takikawa, K.; Kamiya, M.; Nagano, T.; Urano, Y.; Hirose, K. Acidic-PH-Activatable Fluorescence Probes for Visualizing Exocytosis Dynamics. *Angew. Chem., Int. Ed.* **2014**, *53*, 6085−6089.
(57) Caldwell, R. M.; Bermudez, J. G.; Thai, D.; Aonbangkhen, C.; Schuster, B. S.; Courtney, T.; Deiters, A.; Hammer, D. A.; Chenoweth, D. M.; Good, M. C. Optochemical Control of Protein Localization and Activity within Cell-like Compartments. *Biochemistry* **2018**, *57*, 2590−2596.
(58) Chen, X.; Wu, Y.-W. Tunable and Photoswitchable Chemically Induced Dimerization for Chemo-Optogenetic Control of Protein and Organelle Positioning. *Angew. Chem., Int. Ed.* **2018**, *57*, 6796−6799.
(59) Buckley, D. L.; Raina, K.; Darricarrere, N.; Hines, J.; Gustafson, J. L.; Smith, I. E.; Miah, A. H.; Harling, J. D.; Crews, C. M. HaloPROTACS: Use of Small Molecule PROTACs to Induce Degradation of HaloTag Fusion Proteins. *ACS Chem. Biol.* **2015**, *10*, 1831−1837.
(60) Zastrow, M. L.; Huang, Z.; Lippard, S. J. HaloTag-Based Hybrid Targetable and Ratiometric Sensors for Intracellular Zinc. *ACS Chem. Biol.* **2020**, *15*, 396−406.
(61) Deo, C.; Sheu, S.-H.; Seo, J.; Clapham, D. E.; Lavis, L. D. Isomeric Tuning Yields Bright and Targetable Red Ca2+ Indicators. *J. Am. Chem. Soc.* **2019**, *141*, 13734−13738.
(62) Wang, J.; Zhao, Y.; Wang, C.; Zhu, Q.; Du, Z.; Hu, A.; Yang, Y. Organelle-Specific Nitric Oxide Detection in Living Cells via HaloTag Protein Labeling. *PLoS One* **2015**, *10*, e0123986.
(63) Hirata, T.; Terai, T.; Yamamura, H.; Shimonishi, M.; Komatsu, T.; Hanaoka, K.; Ueno, T.; Imaizumi, Y.; Nagano, T.; Urano, Y. Protein-Coupled Fluorescent Probe to Visualize Potassium Ion Transition on Cellular Membranes. *Anal. Chem.* **2016**, *88*, 2693−2700.
(64) Matsui, Y.; Funato, Y.; Imamura, H.; Miki, H.; Mizukami, S.; Kikuchi, K. Visualization of Long-Term Mg2+ Dynamics in Apoptotic Cells Using a Novel Targetable Fluorescent Probe. *Chem. Sci.* **2017**, *8*, 8255−8264.
(65) Gruskos, J. J.; Zhang, G.; Buccella, D. Visualizing Compartmentalized Cellular Mg2+ on Demand with Small-Molecule Fluorescent Sensors. *J. Am. Chem. Soc.* **2016**, *138*, 14639−14649.
(66) Kubánková, M.; Chambers, J. E.; Huber, R. G.; Bond, P. J.; Marciniak, S. J.; Kuimova, M. K. Linker Length Affects Photostability of Protein-Targeted Sensor of Cellular Microviscosity. *Methods Appl. Fluoresc.* **2019**, *7*, 044004.
(67) Popa, I.; Rivas-Pardo, J. A.; Eckels, E. C.; Echelman, D. J.; Badilla, C. L.; Valle-Orero, J.; Fernández, J. M. A HaloTag Anchored Ruler for Week-Long Studies of Protein Dynamics. *J. Am. Chem. Soc.* **2016**, *138*, 10546−10553.
(68) Dahal, N.; Nowitzke, J.; Eis, A.; Popa, I. Binding-Induced Stabilization Measured on the Same Molecular Protein Substrate Using Single-Molecule Magnetic Tweezers and Heterocovalent Attachments. *J. Phys. Chem. B* **2020**, *124*, 3283−3290.
(69) Popa, I.; Berkovich, R.; Alegre-Cebollada, J.; Badilla, C. L.; Rivas-Pardo, J. A.; Taniguchi, Y.; Kawakami, M.; Fernandez, J. M. Nanomechanics of HaloTag Tethers. *J. Am. Chem. Soc.* **2013**, *135*, 12762−12771.
(70) Scull, C. E.; Zhang, Y.; Tower, N.; Rasmussen, L.; Padmalayam, I.; Hunter, R.; Zhai, L.; Bostwick, R.; Schneider, D. A. Discovery of Novel Inhibitors of Ribosome Biogenesis by Innovative High Throughput Screening Strategies. *Biochem. J.* **2019**, *476*, 2209−2219.
(71) Yang, Z.; Weisshaar, J. C. HaloTag Assay Suggests Common Mechanism of E. Coli Membrane Permeabilization Induced by Cationic Peptides. *ACS Chem. Biol.* **2018**, *13*, 2161−2169.
(72) Stüber, J. C.; Kast, F.; Plückthun, A. High-Throughput Quantification of Surface Protein Internalization and Degradation. *ACS Chem. Biol.* **2019**, *14*, 1154−1163.
(73) Deprey, K.; Kritzer, J. A. Quantitative Measurement of Cytosolic Penetration Using the Chloroalkane Penetration Assay. *Methods Enzymol.* **2020**, DOI: 10.1016/bs.mie.2020.03.003.
(74) Peraro, L.; Deprey, K. L.; Moser, M. K.; Zou, Z.; Ball, H. L.; Levine, B.; Kritzer, J. A. Cell Penetration Profiling Using the Chloroalkane Penetration Assay. *J. Am. Chem. Soc.* **2018**, *140*, 11360−11369.
(75) López-Andarias, J.; Saarbach, J.; Moreau, D.; Cheng, Y.; Derivery, E.; Laurent, Q.; González-Gaitán, M.; Winssinger, N.; Sakai, N.; Matile, S. Cell-Penetrating Streptavidin: A General Tool for Bifunctional Delivery with Spatiotemporal Control, Mediated by Transport Systems Such as Adaptive Benzopolysulfane Networks. *J. Am. Chem. Soc.* **2020**, *142*, 4784−4792.
(76) Sato, R.; Kozuka, J.; Ueda, M.; Mishima, R.; Kumagai, Y.; Yoshimura, A.; Minoshima, M.; Mizukami, S.; Kikuchi, K. Intracellular

Protein-Labeling Probes for Multicolor Single-Molecule Imaging of Immune Receptor−Adaptor Molecular Dynamics. *J. Am. Chem. Soc.* **2017**, *139*, 17397−17404.
(77) Foley, C. A.; Potjewyd, F.; Lamb, K. N.; James, L. I.; Frye, S. V. Assessing the Cell Permeability of Bivalent Chemical Degraders Using the Chloroalkane Penetration Assay. *ACS Chem. Biol.* **2020**, *15*, 290−295.
(78) Ballister, E. R.; Aonbangkhen, C.; Mayo, A. M.; Lampson, M. A.; Chenoweth, D. M. Localized Light-Induced Protein Dimerization in Living Cells Using a Photocaged Dimerizer. *Nat. Commun.* **2014**, *5*, 5475.
(79) Li, Y.; Han, X.; Tamm, L. K. Thermodynamics of Fusion Peptide−Membrane Interactions. *Biochemistry* **2003**, *42*, 7245−7251.
(80) Ben-Tal, N.; Ben-Shaul, A.; Nicholls, A.; Honig, B. Free-Energy Determinants of Alpha-Helix Insertion into Lipid Bilayers. *Biophys. J.* **1996**, *70*, 1803−1812.
(81) Van Lehn, R. C.; Alexander-Katz, A. Free Energy Change for Insertion of Charged, Monolayer-Protected Nanoparticles into Lipid Bilayers. *Soft Matter* **2014**, *10*, 648−658.
(82) Behr, J. P.; Kirch, M.; Lehn, J. M. Carrier-Mediated Transport through Bulk Liquid Membranes: Dependence of Transport Rates and Selectivity on Carrier Properties in a Diffusion-Limited Process. *J. Am. Chem. Soc.* **1985**, *107*, 241−246.
(83) Ballister, E. R.; Ayloo, S.; Chenoweth, D. M.; Lampson, M. A.; Holzbaur, E. L. F. Optogenetic Control of Organelle Transport Using a Photocaged Chemical Inducer of Dimerization. *Curr. Biol.* **2015**, *25*, R407−R408.
(84) van den Elsen, J. M. H.; Kuntz, D. A.; Rose, D. R. Structure of Golgi α-Mannosidase II: A Target for Inhibition of Growth and Metastasis of Cancer Cells. *EMBO J.* **2001**, *20*, 3008−3017.
(85) Harduin-Lepers, A.; Mollicone, R.; Delannoy, P.; Oriol, R. The Animal Sialyltransferases and Sialyltransferase-Related Genes: A Phylogenetic Approach. *Glycobiology* **2005**, *15*, 805−817.
(86) Niu, L.; Ma, T.; Yang, F.; Yan, B.; Tang, X.; Yin, H.; Wu, Q.; Huang, Y.; Yao, Z.-P.; Wang, J.; Guo, Y.; Hu, J. Atlastin-Mediated Membrane Tethering Is Critical for Cargo Mobility and Exit from the Endoplasmic Reticulum. *Proc. Natl. Acad. Sci. U. S. A.* **2019**, *116*, 14029.
(87) Huybrechts, S. J.; Van Veldhoven, P. P.; Brees, C.; Mannaerts, G. P.; Los, G. V.; Fransen, M. Peroxisome Dynamics in Cultured Mammalian Cells. *Traffic* **2009**, *10* (11), 1722−1733.
(88) Kirchhausen, T.; Owen, D.; Harrison, S. C. Molecular Structure, Function, and Dynamics of Clathrin-Mediated Membrane Traffic. *Cold Spring Harbor Perspect. Biol.* **2014**, *6*, a016725.
(89) Agrawal, G.; Subramani, S. Emerging Role of the Endoplasmic Reticulum in Peroxisome Biogenesis. *Front. Physiol.* **2013**, *4*, 286.
(90) Fransen, M.; Lismont, C.; Walton, P. The Peroxisome-Mitochondria Connection: How and Why? *Int. J. Mol. Sci.* **2017**, *18*, 1126.
(91) Casares, D.; Escribá, P. V.; Rosselló, C. A. Membrane Lipid Composition: Effect on Membrane and Organelle Structure, Function and Compartmentalization and Therapeutic Avenues. *Int. J. Mol. Sci.* **2019**, *20*, 2167.
(92) van Meer, G.; de Kroon, A. I. P. M. Lipid Map of the Mammalian Cell. *J. Cell Sci.* **2011**, *124*, 5−8.
(93) Jackson, C. L.; Walch, L.; Verbavatz, J.-M. Lipids and Their Trafficking: An Integral Part of Cellular Organization. *Dev. Cell* **2016**, *39*, 139−153.
(94) Miyake, Y.; Kozutsumi, Y.; Nakamura, S.; Fujita, T.; Kawasaki, T. Serine Palmitoyltransferase Is the Primary Target of a Sphingosine-like Immunosuppressant, ISP-1/Myriocin. *Biochem. Biophys. Res. Commun.* **1995**, *211*, 396−403.

https://dx.doi.org/10.1021/acscentsci.0c00666
ACS Cent. Sci. 2020, 6, 1376−1385